Size-dependent properties of CeO_{2-y} nanoparticles as studied by Raman scattering

Jonathan E. Spanier, Richard D. Robinson, Feng Zhang, Siu-Wai Chan, and Irving P. Herman*
Department of Applied Physics and Applied Mathematics, and the Materials Research Science and Engineering Center, Columbia University, New York, New York 10027
(Received 16 April 2001; published 29 November 2001)

The combined effects of strain and phonon confinement are seen to explain why the Raman peak near 464 cm^{-1} in CeO_{2-y} nanoparticles shifts to progressively lower energies and the lineshape of this feature gets progressively broader and asymmetric (on the low-energy side) as the particle size gets smaller. The increasing lattice constant measured for decreasing particle size explains this Raman shift well. The linewidth change is fairly well explained by the inhomogenous strain broadening associated with the small dispersion in particle size and by phonon confinement. The spectra are also likely to be directly affected by the presence of oxygen vacancies. Comparison of the temperature dependence of the Raman lineshape in the nanoparticles and the bulk shows that phonon coupling is no faster in the nanoparticles, so size-dependent phonon coupling does not contribute to the large nanoparticle peak red shifts and broadening at room temperature. Irreversible thermally induced changes are observed in the Raman peak position of the nanoparticles.

DOI: 10.1103/PhysRevB.64.245407 PACS number(s): 63.22.+m, 63.20.Kr, 63.20.Dj

I. INTRODUCTION

CeO_2 is of interest as a catalyst in vehicle emissions systems,[1] for cracking heavy oil in zeolites,[2] as a potentially useful solid oxide fuel cell electrolyte material,[3] and for gas sensors,[4] optical coatings,[5] high-T_c superconductor structures,[6] silicon-on-insulator structures, and high storage capacitor devices.[7,8] Some applications may benefit from using monodisperse CeO_2 nanoparticles, due to either possibly new properties in the nanodimension or the greater control in uniform structures.

Li *et al.*[9] have prepared and characterized monodisperse CeO_2 nanoparticles. Wu *et al.*[10] have used extended x-ray-absorption fine structure to study the local atomic structure around Ce ions in CeO_2 nanoparticles. Electron diffraction has shown that a decrease in the size of CeO_2 nanoparticles is accompanied by a significant increase in the lattice parameter.[11,12] Such changes in lattice constant with particle size have also been confirmed by x-ray diffraction in Ref. 13. The authors in Ref. 12 explained this increase in terms of an associated reduction in the valence of the Ce^{4+} ions to Ce^{3+} ions caused by an increasing molar fraction of oxygen vacancies. In a nanoparticle system that naturally possesses an enormous surface area per unit volume, such vacancies can enhance the ability of a volume of this material to store and release oxygen. When used as an additive to catalysts in automotive emissions systems, these nanoparticles can further enhance the range of fuel/air mixtures at which CO can be oxidized and NO_x can be reduced.

Previous Raman studies of CeO_2 nanoparticles (at room temperature, RT) have demonstrated that the Raman peak energy decreases and the linewidth increases with decreasing particle size. It has been suggested that these dependences be used to measure particle size rapidly. However, Ref. 14 could not explain these dependences using a phonon-confinement model, and suggested that phonon relaxation could be different, i.e., faster, with smaller nanoparticle size and that this could account for the Raman-spectrum changes with size. Some features in the CeO_2 nanoparticles Raman spectrum have been attributed to significant concentrations of impurity atoms or vacancies.[15]

A detailed Raman analysis of CeO_2 nanoparticles is presented here for a range of particle sizes and preparations. The increasing lattice constant (strain relative to the bulk) for successively smaller particles is seen to explain much of the Raman-spectrum changes with particle size, when the dispersion in the particle-size distribution and phonon confinement are also included. If the rate of optical-phonon decay to acoustic phonons or coefficient of thermal expansion at room temperature were to vary with particle size, then the Raman peak energy and linewidth would also vary differently with temperature for different particle sizes. Accordingly, the Raman spectrum is also studied as a function of temperature for different particle sizes.

II. EXPERIMENTAL PROCEDURE

Solutions of $0.04M$ $Ce(NO_3)_3$ and $0.5M$ HMT ($C_6H_{12}N_4$, hexamethylenetetramine) reagents were mixed at room temperature with continuous stirring, producing nucleation and growth of CeO_{2-y} particles. Solutions were allowed to mix for different controlled lengths of time (5–24 h) and then placed in a centrifuge, yielding nanoparticles. The resulting particle size, disperison, and shapes were determined by transmission electron microscopy (TEM). The nanoparticle size was controlled by the length of the reaction time. To obtain the largest particles the mixing reaction was carried out for 12–24 h prior to centrifugation and the particles were then sintered in air at atmosphere at different temperatures (400–800 °C) for 8–16 h.[16] The lattice parameter a was determined from fitting the x-ray diffraction peak position and the mean particle diameter from the peak width using the Scherrer formula, $x_0 = 0.94\lambda/B\cos\theta_B$, where λ is the wavelength of the Cu $K\alpha_1$ line, θ_B is the angle between the incident beam and the reflecting lattice planes, and B is the width (in radians) of the diffraction peak. The size dispersion is approximately Gaussian with a full width at the $1/e^2$ points, Δx, which is 44% of the mean diameter. Further

TABLE I. Preparation conditions, mean particle diameter x_0, lattice parameter a, and estimated vacancy concentration y in CeO_{2-y}.

Sample	Preparation Time (h)	Sintering Temperature (°C)	x_0	a (nm)	y[15,27]
Pellet				0.54087	
A	n/a		~5 μm	0.54087	
B	12	850	~25 nm	0.54087	
C	12	700	~15 nm	0.54131	0.008
D	12	600	~10 nm	0.54152	0.013
E	8	not sintered	~7.4 nm	0.54285	0.038
F	5	not sintered	~6.1 nm	0.54330	0.047

details on the synthesis method, microscopy, and x-ray diffraction results are being reported elsewhere.[13] Commercially purchased (Alfa Aesar) 5 μm CeO_2 powders were also characterized by TEM and x-ray powder diffraction for reference. A summary of the particle preparation and properties is shown in Table I.

Unpolarized Raman scattering was collected in the backscattering configuration from 200 to 1200 cm^{-1} at RT from each powder and from a sintered pellet prepared from the 5 μm particles (''bulk'' material). The 488 nm line of the Ar-ion laser was used, focused to a spot size of ~2 μm with an incident laser power of ~3 mW. Laser heating was shown not to be important, with the Raman intensity remaining linear with incident power up to about 20 mW. The Raman spectra were calibrated using plasma lines of the Ar-ion laser, and the resolution was better than 1 cm^{-1}. Unless reported otherwise, all reported peak intensities, positions, and linewidths are the result of Lorentzian fitting.

Raman scattering was also measured from −190 to 600 °C in air for the 5 μm (*A*), sintered 25 nm (*B*), and unsintered 6.1 nm (*F*) particles. The sample temperature was controlled to within ±0.1 °C by a Linkam Model THMS600 heating/cooling stage. The effect of elevated temperature was analyzed in two ways; in each case possible changes in the particle due to high temperatures were checked by comparing the RT spectra before and after each run. The Raman spectra were collected during the temperature upstroke for each particle. Alternatively, Raman spectra of the 6.1 and 25 nm particles were acquired at RT after temperature cycling. During this cycling, the sample temperature was rapidly increased to a set temperature, maintained there for 5 min, was quickly cooled (~100 °C/min) to RT, and a spectrum was collected. In the next cycle, the sample was then heated to a somewhat higher temperature for 5 min, and so on.

III. EXPERIMENTAL RESULTS

A. Room temperature

The room-temperature Raman spectra from the 6.1, 7.4, 10, 15, 25 nm and 5 μm particles, and the ''bulk'' sintered pellet are shown in Fig. 1(a). The spectrum from the bulk has a weak peak near 261 cm^{-1} that is likely a second-order

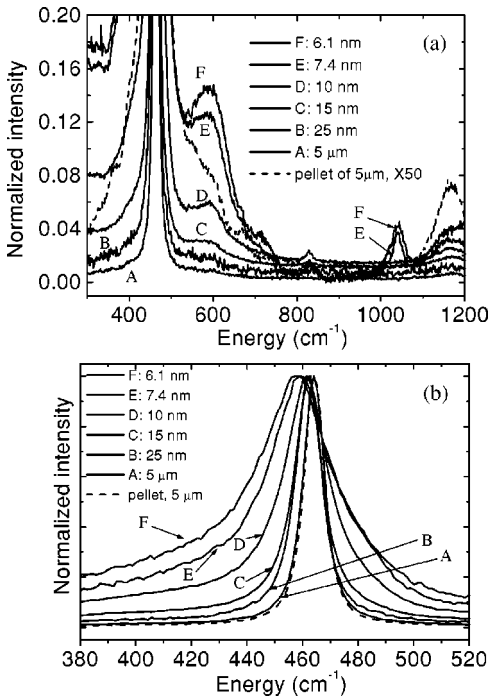

FIG. 1. Normalized Raman spectra from the nanoparticles and the bulk material for (a) the full range of energy studied, and (b) an expanded view of the 464 cm^{-1} peak showing size-dependent changes in the peak position, linewidth, and lineshape.

(2TA) peak, a weak 2TA peak near 368 cm^{-1}, an intense, triply degenerate, first-order peak near 464 cm^{-1}, and two very weak peaks between 550 and 600 cm^{-1}. There are also weak second-order (2LO) peaks near 670 and 1184 cm^{-1}, and a peak near 1277 cm^{-1}. The spectra from the nanoparticles are similar. The 261 cm^{-1} peak still appears, but at slightly lower energy, particularly for the smaller particles. The peak near 560 cm^{-1} is stronger in the nanoparticles (relative to the 464 cm^{-1} peak) than in the bulk. There is also a peak observed in the smaller nanoparticles near 830 cm^{-1} not observed in the bulk. As seen in Fig. 1(b), the 464 cm^{-1} peak shifts to lower energy and asymmetrically broadens with a low-energy shoulder with decreasing particle size.

B. Temperature dependence

The temperature dependence of the 464 cm^{-1} peak position and linewidth for the 6.1 nm, 25 nm, and 5 μm particles is shown in Fig. 2. A decrease in the peak position and increase in the linewidth were observed with increasing temperature in all of these particles. Below RT the temperature dependences of the Raman parameters of these particles are roughly similar except for an offset. Above RT the temperature dependences of the Raman parameters of the 6.1 nm particles appear to be different from those of the larger particles, and the Raman shifts and widths become closer to those for the 25 nm particles. The variation of the Raman peak with temperature for the 7.4 nm particles (not shown) is similar to those for the 6.1 nm particles.

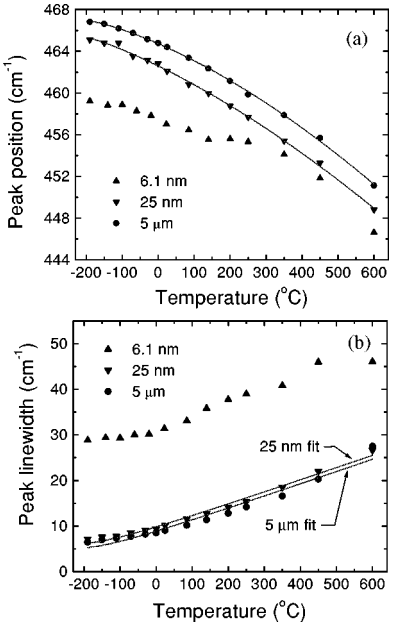

FIG. 2. Measured temperature dependence of the peak (a) position, and (b) linewidth from −190 °C to 600 °C.

Figure 3 shows the peak-position and linewidth for the 6.1 and 25 nm particles measured at RT after 5 min cycling at the depicted elevated temperature. The RT peak position and linewidth do not change for the 25 nm particles following intermittent heating. In contrast, the RT peak position of the 6.1 nm particles increases to progressively higher values following heating to progressively higher temperatures, but the RT linewidth does not change.

IV. MODELS

Several factors can contribute to the changes in the Raman peak position and linewidth of the 464 cm^{-1} peak with nanopartcle size seen in Fig. 1. These include phonon confinement, strain, broadening associated with the size distribution, defects, and variations in phonon relaxation with particle size.

In bulk, defect-free crystalline materials, only $q=0$ phonons can be Raman active and observed. As the dimension and size of a material is reduced, an increasing volume of the reciprocal space is sampled in Raman scattering. Richter *et al.*[17] used a Gaussian weighting function to model Raman scattering at wave vectors away from zone center in low-dimensional materials. For a spherical particle of diameter x, the Raman intensity profile can be approximated by

$$I(\omega,x)\propto\sum\int\frac{\exp\left(\frac{-q^2x^2}{8\beta}\right)}{\{\omega-[\omega_i(q)+\Delta\omega_i(q,x)]\}^2+(\Gamma/2)^2}d^3q, \tag{1}$$

where Γ is the natural Raman full width at half maximum (FWHM), q is the wave vector and, for the time being, $\Delta\omega_i(q,x)=0$. The sum is over the three allowed (and here equally weighted) Raman modes with $\omega_i(q=0)$ $=464.4$ cm^{-1}. $\omega_i(q)$ is the phonon dispersion for the selected mode, represented by parabolic fits to the CeO_2 phonon dispersion curves by Weber *et al.*[14] or Nakajima *et al.*[18] The angular integral in wave vector space in the Brillouin zone is performed by integrating along the Δ, Σ, and Λ symmetry directions, weighting each by the number of equivalent symmetry directions. In the Richter phonon-confinement model $\beta=1$. The alternative Campbell model,[19] in which the phonons are spatially confined even more strongly, can be used by setting $\beta=2\pi^2$.

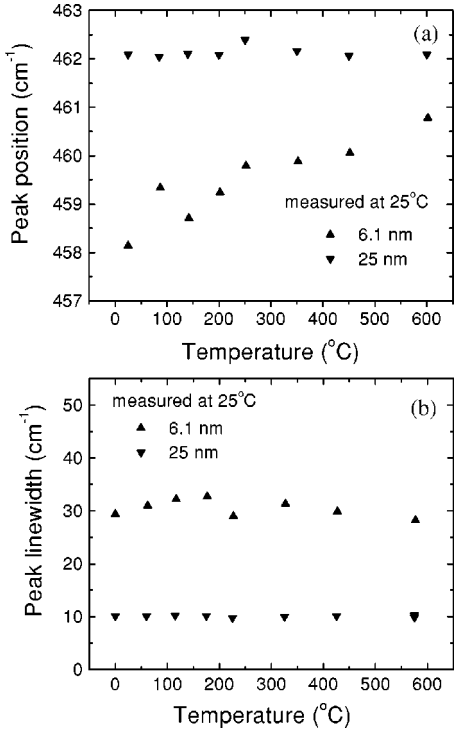

FIG. 3. Changes in the measured, room-temperature peak (a) position, and (b) linewidth following brief temperature cycling (heating) in air to the depicted elevated temperature.

Changes in the lattice parameter with particle size can affect the Raman peak position. The measured variation of lattice parameter a on particle size x is fitted by $a=a_0+k/x^2$ where $k=0.0939$ nm^3, where the bulk value $a_0=0.54087$ nm.[13] Within each particle the strain is taken to be uniform. The change in lattice parameter Δa under a hydrostatic pressure P is $\Delta a/a_0=-P/3B$ where B is the bulk modulus. Therefore, the peak position of the Raman mode centered at ω_i changes by $\Delta\omega_i(q,x)=-3\gamma_i(q)\omega_i(q)\times[\Delta a/a_0]$, where the mode Grüneisen parameter is $\gamma_i=-d\ln\omega_i/d\ln V=(B/\omega_i)(d\omega_i/dP)$. The value of γ_i for the 464 cm^{-1} mode of 1.24, based on Ref. 14, is used here for all modes and q. Using this shifted frequency gives the effect of this average strain alone. To first order, the combined influence of average strain and confinement for particles of size x is obtained by using this $\Delta\omega_i(q,x)$ in Eq. (1).

The dispersion in particle size leads to a dispersion in lattice constants, and, therefore, inhomogeneous strain and broadening. This size distribution for x is approximately a Gaussian centered at the average size x_0 with a Gaussian

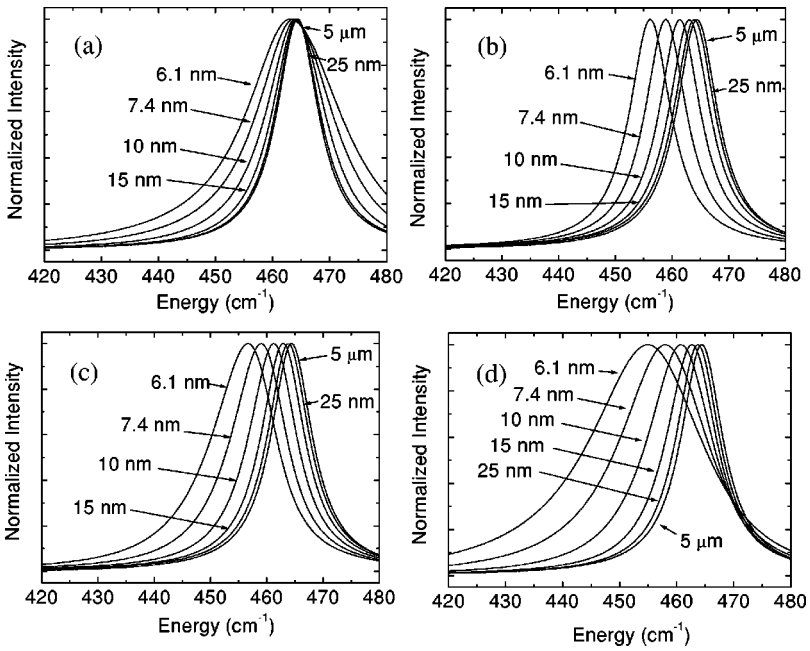

FIG. 4. Model Raman spectra for selected nanoparticle sizes along with the bulk for reference, for (a) confinement only, (b) average strain only, (c) inhomogeneous strain only, and (d) the combination of inhomogeneous strain and confinement. (a) and (d) are shown for the Campbell phonon confinement model ($\beta = 2\pi^2$) using the Nakajima phonon dispersion.

width of $\Delta x = 0.44 x_0$. For each x, the shifted frequency is given above. The effect of this inhomogeneous strain alone is obtained by integrating such shifted spectra over the Gaussian distribution for x. It leads to asymmetric broadening (distorted Gaussian lineshape) and to very little additional peak shift. To first order, the combined effects of inhomogenous strain and confinement are obtained by integrating Eq. (1) over this Gaussian.

Figure 4 shows the model Raman spectra for selected nanoparticle sizes and the bulk with confinement only (using the Campbell model and the Nakajima phonon dispersion curves), average strain only, and combinations of confinement with either average or inhomogeneous strain.

Another source of shifting and broadening is the presence of oxygen vacancies, corresponding to a stoichiometry CeO_{2-y}. McBride *et al.* have calculated the Raman spectra for CeO_2 due to vacancies from phonon density of states calculations based on a rigid-ion model and a model including mass disorder.[15] Using their approach, Fig. 5(a) shows a simulated Raman spectra for selected values of impurity concentrations y corresponding to those in Table I; Fig. 5(b) shows the region near 560 cm^{-1} with an expanded vertical scale. As constructed, this vacancy model provides a shifted peak position but does not provide a concomitant change in linewidth.

Figure 6 shows the Raman peak position and linewidth for the 464 cm^{-1} line as a function of experimental particle sizes for the measured data and models for various combinations of confinement models, average or inhomogeneous strain, and defects. Reference 15 was used to provide the estimates of the vacancy concentration (Table I). This estimate assumes that the strain comes from the presence of Ce^{3+} ions and oxygen vacancies. No other effects, including the effect of surface stress, have been taken into account.[13]

The temperature dependence of the Raman peak position is

$$\omega_p(T) = \omega_0 + \Delta^{(1)}(T) + \Delta^{(2)}(T). \tag{2}$$

The first correction term in Eq. (2) accounts for the effect of thermal expansion; it is

$$\Delta^{(1)}(T) = \omega_0[\exp(-3\alpha\gamma_i T) - 1], \tag{3}$$

where α is the linear coefficient of thermal expansion, which is assumed to be independent of T. It leads to a decrease in

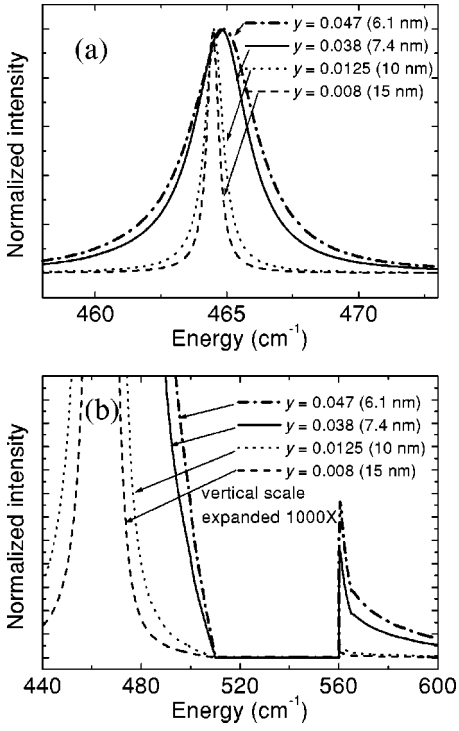

FIG. 5. Simulated Raman spectra for selected impurity concentrations y (a) near 464 cm^{-1} and (b) with an expanded vertical scale and also including the feature near 560 cm^{-1}.

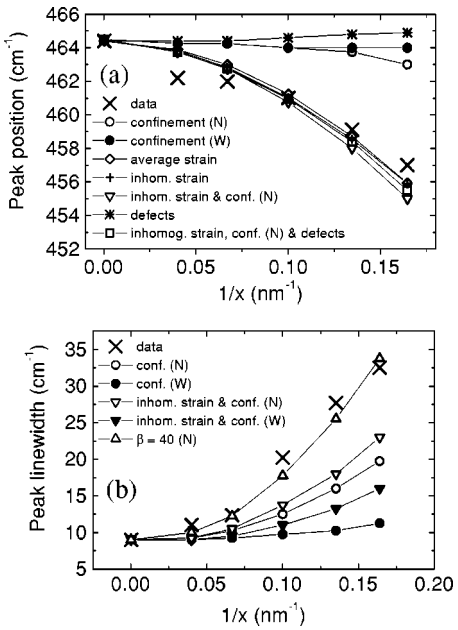

FIG. 6. (a) Peak position and (b) linewidth, respectively, for the 464 cm^{-1} Raman line as a function of particle size for the measured data (denoted by $\times$) and models for confinement only (circles), average strain only (diamonds), inhomogeneous strain only (+), the combination of inhomogeneous strain and confinement (inverted triangles), vacancy defects (asterisks), and the combination of vacancies with inhomogeneous strain and confinement (squares). The open circles and triangles denote results obtained using the Nakajima dispersion with the Campbell model; the solid ones denote results obtained using the Weber dispersion with the Campbell model. In (b) the predictions of the model with combined inhomogeneous strain and confinement are also shown for Nakajima dispersion with the $\beta=40$ confinement model (open inverted triangles).

peak energy $\propto T$ at higher temperature. The second correction is the phonon-phonon coupling term $\Delta^{(2)}(T)$, which describes the anharmonic coupling between phonons, and can be approximated as[20]

$$\Delta^{(2)}(T)=A_1\left\{1+\sum_{j=1}^{2}\frac{1}{(e^{x_j}-1)}\right\}+A_2\left\{1+\sum_{k=1}^{3}\frac{1}{(e^{y_k}-1)}+\frac{1}{(e^{y_k}-1)^2}\right\}. \quad (4)$$

The first term describes the coupling of the optical phonon to two lower-energy phonons (three-phonon coupling, with $x_1=x_2=\hbar\omega_0/2kT$) which is $\propto T$ at higher temperatures, and the second term describes the coupling to three phonons (four-phonon coupling, with $y_1=y_2=y_3=\hbar\omega_0/3kT$) which is $\propto T^2$ at higher temperatures.

One model of the temperature dependence of the Raman linewidth is

$$\Gamma_p(T)=\Gamma_0+\Delta\Gamma(T), \quad (5)$$

where the contribution due to phonon coupling decay is,[20]

TABLE II. Fit parameters for peak shift, in cm^{-1}, alternately using bulk values of α and γ_i, or $\alpha\gamma_i=0$.

Sample	ω_0	A_1	ω_0, $\alpha\gamma_i=0$	A_1, $\alpha\gamma_i=0$
A (5 μm)	469.8±0.5	0.03±0.17	471.2±0.3	−3.7±0.1
B (25 nm)	468.1±0.4	−0.14±0.13	469.4±0.2	−3.8±0.1
F (6.1 nm)	459.3±0.3	1.91±0.52	462.0±0.5	−2.5±0.3

$$\Delta\Gamma(T)=B_1\left\{1+\sum_{j=1}^{2}\frac{1}{(e^{x_j}-1)}\right\}+B_2\left\{1+\sum_{k=1}^{3}\frac{1}{(e^{y_k}-1)}+\frac{1}{(e^{y_k}-1)^2}\right\}. \quad (6)$$

Again, at higher temperatures the first and second terms for this phonon damping term, respectively, vary as T and T^2 at higher temperatures. The first term Γ_0 is due to other types of broadening that do not depend on the thermal population of phonons. This could be instrumental (such as that due to the spectrometer and the charge-coupled device (CCD) array pixel size—here about 1.2 cm^{-1}) and/or intrinsic (such as that due to inhomogeneous strain here, which should depend little on T). In studies of bulk materials, Γ_0 is usually zero if instrumental broadening can be neglected. The linewidths rigorously add as in Eq. (5) only if the lineshape characterized by Γ_0 is Lorentzian, since the contribution of phonon decay, $\Delta\Gamma(T)$, is Lorentzian (LL model). Otherwise, the convolution of the two lineshapes gives a different result. For Gausssian broadening by the Γ_0 term, the resulting lineshape is a Voigt profile with a FWHM linewidth,[21]

$$\Gamma_p(T)=\Delta\Gamma(T)/2+\sqrt{[\Delta\Gamma(T)]^2/4+(\Gamma_0)^2}. \quad (7)$$

Below 100 °C the Raman shift and width curves are roughly similar for the 6.1 nm, 25 nm, and 5 μm particles (except for an offset). Data at all temperatures were used to fit the spectra of the 25 nm and 5 μm particles, while only data at and below RT were used to fit the 6.1 nm particle spectra because of the changes seen at higher T. (The RT measurements in Fig. 3 show that there are irreversible structural changes only in these very small particles.) These peak shift parameters were fit first. Initially α, ω_0, A_1, and A_2 were varied in the fitting, but the observed variation with temperature was found to be capable of fitting only two parameters; consequently, α was set equal to the bulk value $\alpha=1.16\times10^{-5}K^{-1}$ (Ref. 22) and A_2, which should change the curve shape only at very high temperature, was set equal to zero (Table II). This led to very small and sometimes positive values of A_1 even for the bulk samples. This is unexpected and may mean that the value used for γ_i (1.24, Ref. 14) is too large, or at least that the product $\alpha\gamma_i$ is too large—even for the bulk. To help characterize the peak shift data, fits to Eq. (2) were then obtained in the other extreme using $\alpha\gamma_i=0$—with ω_0 and A_1 as free parameters. The linewidths were then fit using Eq. (4) and (5) with Γ_0 and B_1 as the free parameters, using ω_0 from the shift fit and setting B_2 equal to zero (as was A_2). It was assumed that the nonphonon

TABLE III. Fit parameters for the FWHM peak linewidth, in cm^{-1}, using ω_0 from $\alpha\gamma_i=0$ fits from Table II, assuming the temperature-independent (Γ_0) and temperature-dependent (B_1) terms are both Lorentzians (LL) or that the former is a Gaussian and latter is a Lorentzian (voigt profile). For reference, the fits assuming both terms are Gaussian (GG) are also given.

Sample	Γ_0, LL	B_1, LL	Γ_0, Voigt	B_1, Voigt	Γ_0, GG	B_1, GG
A (5 μm)	0.5±0.7	4.7±0.3	2.2±1.0	4.7±0.2	3.1±1.3	4.7±0.2
B (25 nm)	1.5±0.4	4.6±0.1	3.2±0.4	4.9±0.1	4.4±0.4	4.9±0.1
F (6.1 nm)	26.2±0.6	2.5±0.4	26.4±0.5	4.4±0.6	27.9±0.3	7.1±0.5

broadening ("Γ_0" term) was either Lorentzian [Eq. (5) valid, LL] or Gaussian [Voigt profle convolution instead of Eq. (5)] (Table III). These fits are plotted in Fig. 2 using the parameters from the $\alpha\gamma_i=0$, LL fits in Tables II and III.

V. DISCUSSION

The more recent Nakajima phonon-dispersion curves show ω_i varying with q much faster than do the Weber curves for all phonon branches. Both the Richter and Campbell phonon-confinement models predict very little Raman shift with particle size for each phonon dispersion. Using the Campbell confinement model, the increase in Raman linewidth for the 6.1 nm particles is 10.3 cm^{-1} (to a total linewidth of 19.3 cm^{-1}) for the Nakajima dispersion. Including the effect of inhomogeneous strain increases the total width to 23.0 cm^{-1}, compared to the 32.5 cm^{-1} linewidth seen experimentally. For these 6.1-nm-diameter particles, the increase in linewidth due to confinement is only 2.0 cm^{-1} for the Campbell confinement model with Weber dispersion, and $\ll 1$ cm^{-1} for the Richter confinement model with either Nakajima or Weber phonon dispersion. The best agreement of the linewidth with particle size, using confinement and inhomogeneous strain is obtained using $\beta\sim 40$ with the Nakajima dispersion. The Richter ($\beta=1$) and Campbell ($\beta=2\pi^2 \sim 20$) models of phonon confinement are based on fairly arbitrary (and different) assumptions about the spatial extent of phonons in confined structures. If the Nakajima phonon dispersions are correct, models with $\beta\sim 40$ represent an even higher degree of phonon confinement than that in the Campbell model, which may be more appropriate for CeO_2. While using phonon dispersion only along the symmetry directions in Eq. (1) may seem to be a limitation, the main features of the predictions do not seem to be very sensitive to this approximation, and are much more sensitive to the choice of phonon dispersion and the degree of phonon confinement.

It is clear from Fig. 6 that the change in the measured 464 cm^{-1} peak position to lower energy with decreasing particle size is more than that expected from any of the confinement models alone, but a bit less than that due to strain alone. [As seen in Fig. 6(a), there is very little difference in the model peak position between the average and inhomogeneous strain alone]. Vacancies increase the peak frequency a bit, progressively more so for smaller particle sizes with concomitant increasing vacancy concentration. The overall change in Raman shift with particle size due to all of these effects is shown in Fig. 6. There is very good agreement with the experimental peak position when strain alone is considered. Agreement is still good, but less perfect, when the effects of confinement and defects are included. Overall, it is seen that strain plays the most significant role.

Together, inhomogeneous strain and confinement can account for much of the broad and asymmetric character of the observed asymmetric lineshapes, and more than that accounted for in earlier work.[14] Inhomogeneous strain is clearly important to the linewidth. Model agreement is good when the more restricted Campbell spatial confinement of phonons is assumed with Nakajima phonon dispersion. When either the less restrictive Richter phonon-confinement model is used and/or the less dispersive Weber phonon dispersion is used, very little broadening due to phonon confinement is seen. Linewidth changes due to vacancies may also be significant. This variation of lattice parameter with particle size may well be due to the changing density of vacancies. It and the actual vacancy density are likely dependent on the details of sample preparation, and as such the use of Raman shifts and linewidths as a diagnostic of particle size should be limited to a given preparation method.[23]

The variations of the phonon frequency and linewidth up to RT definitively show that phonon coupling is not the reason for the increasing peak red shift and broadening with decreasing particle size. If enhanced phonon coupling in the nanoparticles were the reason for these lineshape changes, then the nanoparticle shift and width at low temperature would be relatively much closer to those for the larger particles.

The magnitude of A_1 is smaller for the 6.1 nm particles (2.5 cm^{-1}) than for the 25 nm particles and the bulk ($\sim$3.7 cm^{-1}) for the $\alpha\gamma_i=0$ fits. This would suggest that either phonon coupling or the $\alpha\gamma_i$ product is smaller (or both are smaller) in the nanoparticle than in larger particles. The fits in Table II show that there is some doubt even about the bulk values of $\alpha\gamma_i$, since the value for A_1 in the bulk is suspect. Either the Grüneisen parameter is wrong, or α and γ_i depend on the vacancy concentration. The contribution of thermal expansion used in Eq. (3) assumes that the expansion coefficient does not depend on temperature; this seems to be a good approximation.[3] In any case, it is hard to untangle any potential size-related effects in the peak shift due to thermal expanision and phonon coupling.

The effect of phonon coupling alone is seen in the linewidth. The phonon coupling term B_1 is about 4.7 cm^{-1} for both the 25 nm particles and the bulk, independent of the fit. Reference 24 observed a similar dependence on T in bulk CeO_2. For the 6.1 nm nanoparticles, B_1 is 2.5 cm^{-1} for the

LL fit and 4.4 cm^{-1} for the Voigt fit, respectively, assuming Lorentzian and Gaussian profiles for the nonphonon broadening term; the latter value is close to the bulk value. The Raman lineshapes of the nanoparticles are seen to be more Lorentzian than Gaussian at each temperature, so the former value may be more meaningful, but this is not certain. (The nonphonon coupling contribution would be expected to have a skewed Gaussian lineshape resulting from inhomogeneous broadening, if this strain broadening accounted for all of the low-temperature linewidth). Overall, the parameters in Tables II and III suggest that phonon coupling is no stronger in the CeO_{2-y} nanoparticle than in larger-dimension material, and only possibly that it is somewhat weaker.

This is contrary to the conclusions of Raman studies of nanocrystalline Si films[17,25] and CdSe nanocrystals in glass,[26] which suggest more coupling in the nanodomains than in larger domains. In fitting their lineshapes, Ref. 25 used a LL fit, while Refs. 17 and 26 used $\Gamma_p(T) = \sqrt{(\Gamma_0)^2 + [\Delta\Gamma(T)]^2}$, which assumes that both broadening terms are Gaussian (GG model). Table III also gives the fits for Raman scattering in CeO_{2-y} for a GG fit. This leads to $B_1 = 7.1$ cm^{-1} for the 6.1 nm particles, which would suggest that phonon decay broadening is faster in the nanoparticle. Since the phonon lifetime broadening is definitely Lorentzian, this is not an acceptable possibility. It is emphasized that it is critical to use the proper lineshapes to obtain broadening fits, especially when the low-temperature width is larger than the phonon damping width at most temperatures.

Figure 3 shows a change in the ambient temperature peak position of the 464 cm^{-1} peak after brief heating for the 6.1 nm particles, but not for the 25 nm particles; no change in ambient temperature linewidth is seen for either. These observations are consistent with strain relaxation in the 6.1 nm particles, since strain is the major contributor to the Raman shift. Since the heating times were too short for particle growth from sintering, heating should change the linewidth relatively little, as is seen here, since phonon confinement is a very important contribution to the linewidth for nanoparticles here.

We considered applying the above analysis to other Raman peaks. In contrast to the changes of the 464 cm^{-1} phonon line, the $\sim$280 cm^{-1} peak increases in energy very slightly for decreasing particle size. Based on the phonon dispersion in Ref. 14, the shift and asymmetric broadening due to confinement in the $\sim$280 cm^{-1} line is expected to be opposite to that of the 464 cm^{-1} line, while the direction of the shift due to strain would be the same. The value of γ_i for the $\sim$280 cm^{-1} line has not been reported. The Raman signal is too weak in three of the particle sizes to determine the peak position and linewidth well enough.

The peak observed near 560 cm^{-1} has been attributed to the presence of defects (impurities and/or vacancies).[15] This peak is observed in all of the nanoparticles, but is several orders of magnitude weaker in the bulk. The peak near 830 cm^{-1} appears in CeO_2 nanoparticles of all sizes, but never in either the 5 μm particles or the sintered pellet. It has not been reported in previous Raman investigations of nanoparticle CeO_2. It could be due to a second-order phonon, a local mode centered on vacancies, or the presence of another elemental species.

VI. CONCLUDING REMARKS

The peak position of the strong, triply degenerate, first-order Raman line in CeO_{2-y} at 464 cm^{-1} is shifted to progressively lower energies as the particle size gets smaller, and the peak gets progressively broader and asymmetric on the low-energy side. The increasing lattice constant with decreasing particle size explains this Raman shift well. The linewidth change is fairly well explained by the inhomogenous strain broadening associated with dispersion in particle size and by phonon confinement. The spectra are also likely to be directly affected by the presence of vacancies. Phonon coupling is not enhanced in the nanoparticle compared to larger particles, so it is not the source of the Raman peak red shift and broadening with smaller particle size. Irreversible changes in the room temperature Raman peak position in the smaller nanoparticles are seen after heating them for short times above room temperature. This may involve strain relaxation and/or oxygenation. A more detailed study of annealing and processing these particles will be presented elsewhere.

ACKNOWLEDGMENTS

This work was supported primarily by the MRSEC Program of the National Science Foundation under Award Number DMR-9809687. R.D.R. acknowledges support by the Ford Foundation.

*Email address: iph1@columbia.edu

[1] Y.F. Yao and J.T. Kummer, J. Catal. **106**, 307 (1987); E.C. Su, C.N. Montreuil, and W.G. Rothschild, Appl. Catal. **17**, 75 (1985); H.S. Gandhi, A.G. Piken, M. Shelef, and R.G. Delosh, SAE paper #760201 (1976).

[2] T.M. Tri, J. Massardier, P. Gallezot, and B. Imelik, in *Proceedings of the 7th International Congress on Catalysis*, edited by T. Seiyama and K. Tanabe (Elsevier, Amsterdam, 1980), p. 266.

[3] M. Mogensen, N.M. Sammes, and G.A. Tompsett, Solid State Ionics **127**, 63 (2000).

[4] R. Bene, I.V. Perczel, F. Reti, F.A. Meyer, M. Fleisher, and H. Meixner, Sens. Actuators B **71**, 36 (2000); U. Lampe, J. Gerblinger, and H. Meixner, *ibid.* **7**, 787 (1992).

[5] G. Haas, J.B. Ramsey, and R. Thun, J. Opt. Soc. Am. **48**, 324 (1957).

[6] A. Walkenhorst, M. Schmitt, H. Adrian, and K. Petersen, Appl. Phys. Lett. **64**, 1871 (1994).

[7] T. Chikyow, S.M. Bedair, L. Tye, and N.A. El-Masry, Appl. Phys. Lett. **65**, 1030 (1994).

[8] A.H. Morshed, M. Tomita, N. El-Masry, P. McLarty, N.P. Parikh, and S.M. Bedair, in *Epitaxial Oxide Thin Films II*, edited by D. K. Fork, J.S. Speck, I. Shiosaki, and R.M. Wolf, Mater. Res. Soc. Symp. Proc. **401** (Materials Research Society, Pittsburgh, 1996).

[9] F. Li, X. Yu, H. Pan, M. Wang, and X. Xin, Solid State Sci. **2**, 767 (2000).

[10] Z. Wu, L. Guo, H. Li, Q. Yang, Q. Li, and H. Zhu, Mater. Sci. Eng., A **286**, 179 (2000).
[11] S. Tsunekawa, R. Sahara, Y. Kawazoe, and K. Ishikawa, Appl. Surf. Sci. **152**, 53 (1999).
[12] S. Tsunekawa, K. Ishikawa, Z.-Q. Li, Y. Kawazoe, and Y. Kasuya, Phys. Rev. Lett. **85**, 3440 (2000).
[13] F. Zhang, S.-W. Chan, J.E. Spanier, E. Apak, R.D. Robinson, and I.P. Herman, Appl. Phys. Lett. (in press).
[14] W.H. Weber, K.C. Hass, and J.R. McBride, Phys. Rev. B **48**, 178 (1993).
[15] J.R. McBride, K.C. Hass, B.D. Poindexter, and W.H. Weber, J. Appl. Phys. **76**, 2435 (1994).
[16] The particles were sintered in air and the thermal ramping (both increase and decrease) was 100 °C/h and the temperature was maintained at its maximum value for 30 min.
[17] H. Richter, Z.P. Wang, and L. Ley, Solid State Commun. **39**, 625 (1981).
[18] A. Nakajima, A. Yoshihara, and M. Ishgame, Phys. Rev. B **50**, 13 297 (1994); K. Clausen, W. Hayes, J.E. Macdonald, R. Osborn, P.G. Schnabel, M.T. Hutchings, and A. Magerl, J. Chem. Soc., Faraday Trans. 2 **83**, 1109 (1987).
[19] I.H. Campbell and P.M. Fauchet, Solid State Commun. **58**, 739 (1986).
[20] M. Balkanski, R.F. Wallis, and E. Haro, Phys. Rev. B **28**, 1928 (1983).
[21] E.E. Whiting, J. Quant. Spectrosc. Radiat. Transf. **8**, 1379 (1968).
[22] R.G. Schwab, R.A. Steiner, G. Mages, and H.J. Beie, Thin Solid Films **207**, 288 (1992).
[23] G.W. Graham, W.H. Weber, C.R. Peters, and R. Usman, J. Catal. **130**, 310 (1991).
[24] T. Sato and S. Tateyama, Phys. Rev. B **26**, 2257 (1982).
[25] P. Mishra and K.P. Jain, Phys. Rev. B **62**, 14 790 (2000).
[26] A. Tanaka, S. Onari, and T. Arai, Phys. Rev. B **45**, 6587 (1992).
[27] The vacancy concentrations were taken from Ref. 15, assuming Ce^{4+} and Ce^{3+} ionic radii of 0.97 Å and 1.143 Å, respectively.